Frequency response optimization of P-I-N photodiode based on InGaAsN lattice matched to GaAs for High-Speed photodetection applications

R. Amraoui, Abdelkader Aissat, Jean-Pierre Vilcot, Didier Decoster

Version of Record: https://www.sciencedirect.com/science/article/pii/S0030399221005569
Manuscript_769b70fe9cffa7ec03c9fdbed80da365

Frequency Response Optimization of P-I-N Photodiode Based on InGaAsN Lattice Matched to GaAs for High-Speed Photodetection Applications

R.Amraoui[1], A.Aissat[1,2,*], J.P. Vilcot[2], D.Decoster[2]
[1]Faculty of Technology, University of Blida 1 BP270, 09000, Algeria.
[2]Institut d'Electronique, de Microelectronique et de Nanotechnoloie (IEMN), UMR CNRS 8520, Université des Sciences et Technologies de Lile 1, Avenue Poincare, BP60069, 59652 Villeneuve d'Ascq, France.
e.mail1: sakre23@yahoo.fr
email 2: aa_aissat@univ-blida.dz

Abstract

This paper reports on pin photodiode frequency response optimization based on $In_xGa_{1-x}As_{1-y}N_y$ quaternary lattice matched to GaAs. Two transparent layers are placed on p-side and n-side in order to manage the photodiode frequency response limitations. The lattice matching condition is calculated in order to obtain stable structure. The physical and optical parameters calculations are performed at room temperature showing the impact of nitrogen on the absorption coefficient. A stable structure, having 2 % of nitrogen and 6% of indium, allows to achieve a cutoff frequency of about 116GHz and a capacitance of 5.21fF while the quantum efficiency is 41.59% for a depletion region thickness of about 0.55µm. However, in case of depletion region thickness of about 0.625µm, the cutoff frequency degrades to 98GHz while the capacitance diminishes to 4.58fF and the quantum efficiency increases to 51.56%. In addition, a comparative study with literature results has been carried out in order to show the advantages of the proposed photodiode. This comparison affirms that the proposed photodiode based on InGaAsN lattice matched to GaAs exhibits high-speed photo-detection. This work allowed us to obtain a p-i-n photodiode with stable structure suitable for photo-detection at 1.15µm.

Keywords: $In_xGa_{1-x}As_{1-y}N_y$ quaternary, p-i-n photodiode, stable structure, high-speed photo-detection.

1. Introduction

Nowadays, optoelectronic devices such as p-i-n photodiode become more controversial and sophisticated regarding the enormous progress in optical systems. Heterostructures, those based on III–V quaternaries have taken advantage of this development and become a major candidate in optoelectronic devices thanks to their attractive physical and optical properties. Among them, InGaAsN is considered as a promising compound for optoelectronic devices. Since the last few years, InGaAsN deposed on GaAs substrate has received an intense interest in several researches [1-9]. This is due to, firstly, the beneficial applications such as solar cells [10-12],

photo-detection [13] and laser applications [14, 15]. Secondly, the fact that InGaAsN can be grown lattice matched to GaAs [16, 17]. The lattice matched structure has been adopted in different works [18-22].

On the other side, p-i-n photodiode is considered as a pertinent device in modern optical communication systems because of the remarkable characteristics such as high-speed photo-detection. The latter is well assessed in the photodiode frequency response simulation.

The photodiode frequency response calculation has been extensively tackled in quite number of researches. P-I-N photodiode frequency response has been calculated and optimized [23] using an absorbent region made of $In_{0.5}Ga_{0.5}N$ and a single transparent layer on n-side. An analytical model is presented in [24] in order to accurately study the performances of InGaAs/InP based pin photodiode. In ref [25] a formulation was developed for carrier transport using vertical pin photodiode. Author studied the device high frequency response and cleared up its limiting parameters. Recently, author in ref [26] developed a multiple quantum wells InGaN/GaN based pin photodiode in the aim of fabricating high-speed pin photodiode. A p-i-n photodiode was designed [27] with structure consists of: $In_{0.1}Ga_{0.9}N$ as an absorbent region having a thickness of 0.1µm placed between two layers p-type and n-type made of GaN, their thicknesses are 0.1 µm, and 0.3µm respectively. The achieved cutoff frequency was 400MHz, however for an intrinsic region thickness of 1.5µm, the cutoff frequency attained 4GHz. A new analytical model was developed in order to study the p-i-n photodiode high-frequency performance [28]. In Ref [29] a characterization of high-speed large-area p-i-n photodiodes was tackled. Author has proposed a fully analytic model in order to study the frequency response for a homo-structure p-i-n photodiode. P-I-N photodiode having dual-depletion region has been proposed in order to improve the bandwidth [30,31] taking into consideration the transit time and the capacitance effect. Finally, p-i-n photodiode frequency response was calculated analytically in [32].

It is crucial to note that p-i-n photodiode frequency response is mainly limited by two parameters of upmost importance [23-31]: the carriers' transit time and capacitance effect.

The main aim of this research is to obtain a high-speed p-i-n photodiode based on stable structure with low capacitance effect and short transit time. However, in case of conventional photodiode low capacitance effect needs thick absorbent region. This leads to increase the transit time and consequently tends to slow the photodiode response. While, high-speed communications (cutoff frequency >60GHz) need short transit time [33] and low capacitance effect. The influence of both transit time and capacitance effect on the photodiode performances is well shown in the frequency response. In attempt to overcome this issue, a structure based on two transparent layers under field inserted on p-side and n-side of the absorbent region is proposed. In this paper

we have assumed that carriers move at their saturation velocities, so the transit time becomes directly proportional to depletion region the thickness.

In the paper in hand, physical and optical calculations as well as the frequency response optimization for p-i-n photodiode are provided. The photodiode is based on $In_xGa_{1-x}As_{1-y}N_y$ quaternary as an absorbent region lattice matched to GaAs substrate using two transparent layers placed on p-side and n-side. In the first step, the lattice matching condition is calculated in order to obtain stable structure. After that, the bandgap energy as well as the absorption coefficient are calculated at room temperature showing the impact of nitrogen concentration (y) on the absorption coefficient. The next section, on one side, it deals with calculation of the frequency response which corresponds to the transit behavior with highlighting the influence of the absorption coefficient in order to select indium (x) and nitrogen concentrations required in the detection part. On the other side, it deals with the frequency response optimization and the impact of the transit time and the capacitance effect on the frequency response. At a later stage, a comparative study with literature results is provided to evaluate, in term of speed, the benefits of the proposed structure based on InGaAsN lattice matched to GaAs. The next section focuses on the capacitance effect which has a strong impact on the total frequency response. The last section is devoted to the total frequency response and its limitations.

2. Theoretical framework

This study is based on $In_xGa_{1-x}As_{1-y}N_y$ lattice matched to GaAs which allows to obtain a stable structure i.e. $\varepsilon(x,y) = 0$, where $\varepsilon(x,y)$ represents the strain given by [13,34,35]:

$$\varepsilon(x,y) = \frac{a_s - a_e(x,y)}{a_e(x,y)} \quad (1)$$

where:

a_s: is the lattice parameter of the substrate.

$a_e(x,y)$: is the lattice parameter of $In_xGa_{1-x}As_{1-y}N_y$.

The variation of the strain $\varepsilon(x,y)$ as a function of indium and nitrogen concentrations is illustrated in figure.1.

After calculation, the condition that allows to obtain a stable structure is:

$$y(x) = \frac{0.40.x}{1.15 - 0.075.x} \quad (2)$$

Equation.2 presents the variation of nitrogen concentration as a function of indium concentration. For each pair (x, y) we have a stable structure.

Indeed, the introduction of small quantity of nitrogen into InGaAs semiconductor results a drastic reduction in the bandgap energy. This is due to strong interaction between the conduction band and spatially localized state of nitrogen (E_N) [36]. Consequently, the conduction band splits into two subbands E_+ and E_-. Increasing the amount of nitrogen results a repulsion of E_+ and E_- above and below respectively, which has a significant effect on optical properties. The bandgap reduction due to nitrogen incorporation is well clarified by the Band Anti-Crossing model (BAC) [13, 37-41]:

$$E_{\mp} = \left[(E_N + E_M) \mp \sqrt{(E_N - E_M)^2 + 4V_{MN}{}^2}\right] \quad (3)$$

$$E_N = 1.52 - 3.9y \quad (4)$$

$$E_M = E_0 - 1.55\ eV + \frac{h^2}{2m_e^*} \quad (5)$$

$$V_{MN} = b_{MN}\sqrt{y} \quad (6)$$

where:

b_{MN}=2.3.

E_o: the conduction band minimum of InGaAs.

m^*_e : is electron effective mass in the ternary InGaAs.

E_M: is the energy of the InGaAs matrix conduction band edge.

E_N: is the nitrogen energy level relative to the top of the valence band.

V_{MN}: is the matrix element describes the interaction between E_M and E_N.

In the equation.3 only E_- is taken into account, because E_- is responsible for the reduction in bandgap energy [42,43].

Absorbing photons energy to generate electrical signal is the basic role of the photodiode. If an incident optical beam having an energy hυ smaller than the semiconductor bandgap, the device appears as transparent to the photons energies, therefore photons are not absorbed. By contrast, if hυ is greater than or equal to the bandgap energy, electrons in the valence band absorb the photons energies and move towards the conduction band. The absorption coefficient α(E) in case of absorbed photons is given as follow [34,44-45]:

$$\alpha(E) = \alpha_0 \cdot \frac{\sqrt{E - E_g(x,y)}}{E} \quad (7)$$

where:

E: is the photon energy.

α_o: constant depends on the semiconductor.

$E_g(x,y)$: is the bandgap energy of $In_xGa_{1-x}As_{1-y}N_y$.

To perform the frequency response calculation, we have assumed that carriers move with their saturation velocities given by [46-51] at 300K for binary compounds (InAs, GaAs, InN, GaN) and the saturation velocity of InGaAsN can be determined by using Vegard's law.

The total current circulates in the device is given as follow [23].

$$i(t) = B\left[v_p \cdot P(t) + v_n \cdot N(t)\right] \tag{8}$$

where

$$B = \frac{q}{d_t},$$

q is the electron charge, d_t is the depletion region thickness.

v_p, v_n are holes and electrons saturation velocities respectively.

P(t) and N(t) represent the number of holes and electrons in the depletion region.

Light-generated carriers transit from the absorbent region towards p-type and n-type regions. Holes response is completed after abandoning the depletion region in duration of $d_p/v_p + d_{abs}/v_p$ and electrons in duration of $d_n/v_n + d_{abs}/v_n$. The carriers' contributions are:

- for holes:

$$i_p(t) = \frac{q v_p p_0 A}{\alpha \cdot dt} \cdot \left[\frac{e^{\alpha \cdot d_{abs}} - 1}{e^{\alpha \cdot d_{abs}}}\right] \frac{e^{\alpha \cdot d_{abs}} - 1}{e^{\alpha \cdot d_{abs}}} \quad 0 < t < \tau_p \tag{9}$$

$$i_p(t) = \frac{q v_p p_0 A}{\alpha . d_t} \cdot \left[\frac{e^{\alpha \cdot d_{abs}} - e^{\alpha(v_p \cdot t - d_p)}}{e^{\alpha(v_p t - d_p + d_{abs})}}\right] \quad \tau_p < t < \tau_p + \tau_{p,abs} \tag{10}$$

- for electrons:

$$i_n(t) = \frac{q v_n n_0 A}{\alpha \cdot d_t} \cdot \left[\frac{e^{\alpha \cdot d_{abs}} - 1}{e^{\alpha \cdot d_{abs}}}\right] \quad 0 < t < \tau_n \tag{11}$$

$$i_n(t) = \frac{q v_n n_0 A}{\alpha \cdot d_t} \cdot \left[\frac{e^{\alpha(v_n \cdot t - d_n + d_{abs})} - 1}{e^{\alpha(v_n \cdot t - d_n + d_{abs})}}\right] \quad \tau_n < t < \tau_n + \tau_{n,abs} \tag{12}$$

where:

$\tau_{n,abs} = d_{abs}/v_n$, $\tau_n = d_n/v_n$ and $\tau_{p,\,abs} = d_{abs}/v_p$, $\tau_p = d_p/v_p$.

p_o and n_o represent the carriers maximum densities.

d_{abs} is the absorbent region thickness.

d_p(d_n) is p-side (n-side) transparent layer thickness.

$\tau_{p,abs}$($\tau_{n,abs}$) is the transit time required for holes (electrons) to cross the absorbent region.

τ_p(τ_n) are the transit time that holes(electrons) take to cross the p-side (n-side) transparent layer.

A is the junction area.

The impulse response is the sum of the electrons and holes contributions, it is given as:

$$g(t) = B' \cdot \left[i_p(t) + i_n(t)\right] \tag{13}$$

where

$$B' = \frac{1}{q \cdot N_{opt}}$$

N_{opt} is the photons number in the optical beam.

The frequency response allows to verify the photodiode performance. From the photodiode impulse response, we are able to obtain the frequency response by using the Fourier transform:

$$G_p(w) = \frac{v_p}{j \cdot d_t \cdot w} \cdot \left(1 + j \cdot \frac{a_1}{a_2} \cdot \frac{e^{j\cdot(a_2 - j\cdot a_4)} + e^{-j\cdot(a_2 + j\cdot a_4)}}{e^{a_1} - e^{-a_1}}\right) \tag{14}$$

$$G_n(w) = \frac{v_n}{j \cdot d_t \cdot w} \cdot \left(1 + j \cdot \frac{a_1}{a_3} \cdot \frac{e^{j\cdot(a_3 - j\cdot a_5)} + e^{-j\cdot(a_3 + j\cdot a_5)}}{e^{a_1} - e^{-a_1}}\right) \tag{15}$$

where

w is the angular frequency.

$a_1 = \frac{\alpha \cdot d_{abs}}{2}$, $a_2 = \frac{d_{abs}}{2} \cdot \left(\frac{w}{v_p} - j \cdot \alpha\right)$, $a_3 = \frac{d_{abs}}{2} \cdot \left(\frac{w}{v_n} + j \cdot \alpha\right)$, $a_4 = -j \cdot \frac{w}{v_p} \cdot \left(\frac{d_{abs}}{2} + d_p\right)$, $a_5 = -j \cdot \frac{w}{v_n} \cdot \left(\frac{d_{abs}}{2} + d_n\right)$.

3. Nitrogen impact on optical behavior

The first step is to calculate the bandgap energy and the absorption coefficient. The pairs (x, y) are extracted from equation.2. Indium concentration is limited at 14% and therefore nitrogen concentration is limited at 4.96%. The evolution of the absorption coefficient versus nitrogen concentration is presented in figure.2 in which some nitrogen concentrations match the stable structure are provided.

The influence of nitrogen on the absorption coefficient is well clarified in figure.2. A slight concentration of nitrogen results a notable reduction in the bandgap energy, consequently a considerable amelioration in the absorption coefficient (α). For example, in case of y=2% the bandgap energy is about 1.08eV and the absorption coefficient is ~~of~~ about $\alpha = 4.72 \times 10^4 cm^{-1}$. However, for y=2.5% the bandgap energy decreases to 1.03eV, while the absorption coefficient rises to $\alpha = 4.44 \times 10^5\ cm^{-1}$.

The physical and optical properties of $In_xGa_{1-x}As_{1-y}N_y$ lattice matched to GaAs for $6\% \leq x \leq 7\%$ and $2\% \leq y \leq 2.5\%$ are as follow: bandgap energy from 1.08eV down to 1.033eV, the photo-detection wavelength from 1.15µm until 1.20µm and the absorption coefficient ranging from $4.72 \times 10^4\ cm^{-1}$ to $4.44 \times 10^5 cm^{-1}$.

4. PIN photodiode frequency response optimization

The proposed structure is provided in figure.3. It consists of: n-type GaAs layer followed by the first under field transparent layer made of GaAs having a thickness of d_n(µm). The absorbent region is an intrinsic $In_xGa_{1-x}As_{1-y}N_y$ with thickness of d_{abs}(µm) and the second under field transparent layer is made of GaAs having a thickness of d_p(µm). Finally, the p-type layer is made of GaAs. The cathode and anode contacts are made of Ti/Al/Ni/Au and Ni/Au respectively to guarantee the connection with the electrical circuit.

According to the previous results, two configurations satisfying the stable structure have been adopted taking indium cost and nitrogen influence into consideration. The first configuration is the quaternary $In_{0.07}Ga_{0.93}As_{0.975}N_{0.025}$, while the second is $In_{0.06}Ga_{0.94}As_{0.98}N_{0.02}$. The physical and optical parameters of these two configurations are given in section 3.

Focusing on the link between the cutoff frequency and the absorption coefficient, different absorbent regions thicknesses have been examined using the first configuration ($In_{0.07}Ga_{0.93}As_{0.975}N_{0.025}$): d_{abs}=0.5, 0.8 and 1µm, while both d_p and d_n are kept at 0.5µm. The results are as follow: for d_{abs}=0.5µm the cutoff frequency at -3 dB is 67.46GHz, this value is unchanged either for d_{abs}=0.8µm or 1µm. The cutoff frequency seems stuck at 67.46GHz despite using different absorbent region thicknesses. This is due to the high absorption coefficient caused by the important nitrogen concentration which has a strong impact on the bandgap energy.

The same study is applied on the second configuration: $In_{0.06}Ga_{0.94}As_{0.98}N_{0.02}$ which has a reduced absorption coefficient compared to the first configuration. The results are established in figure.4. According to this figure, for d_{abs}=0.2µm the structure reveals a -3dB cutoff frequency of 59.00GHz, then the cutoff frequency degrades to 49.03GHz for d_{abs}=0.5µm. Whereas, in case of the absorbent region is sufficiently large, d_{abs}=0.8 and 1µm, the cutoff frequency reduces to 44.33GHz and 42.86GHz respectively. On the other hand, figure.4 affirms that the cutoff frequency depends highly on the absorbent region thickness when using low absorption coefficient (order of 10^4). For this reason, the second configuration ($In_{0.06}Ga_{0.94}As_{0.98}N_{0.02}$) is selected.

The next step is dedicated to search the optimal depletion region thickness that improves the photodiode frequency response taking into account carriers' transit time and capacitance effect. Figure.5 depicts the cutoff frequency values variation as function of d_p where d_{abs} ranging from 0.1 to 0.4µm, and d_n=0.2, 0.5µm. Figure.6 provides the cutoff frequency values variation as function of d_n where d_{abs} ranging from 0.1 to 0.4µm, while d_p=0.5, 0.375 µm in figure.6.a and d_p=0.2µm in figure.6.b.

According to figure.5, in case d_n=0.2µm (dashed curves) the maximum cutoff frequency is 143GHz, this is given when d_p=0.15µm and d_{abs}=0.1µm. After that, the cutoff frequency decreases to 116.20GHz for

d_p=0.15µm and d_{abs}= 0.2µm, then it degrades to 98.4GHz for d_p=0.125µm and d_{abs}=0.3µm. The last depletion regions have approximately the same transparent layers thicknesses but different absorbent regions which enhance the quantum efficiency as 25.62% for d_{abs}=0.1µm to 41.59% in case d_{abs}=0.2µm until 51.56% for d_{abs}=0.3µm.

Still in figure.5, in case d_n=0.5µm (solid curves) the structure exhibits low cutoff frequencies. The maximum cutoff frequency is about 66.23GHz which is obtained for d_p=0.375µm and d_{abs}=0.1µm. This degradation in the cutoff frequency values is due to increasing the depletion region thickness. This fact leads to reducing the capacitance, but at the same time a long transit time which slows the photodiode response.

Referring to figure.6.a, when d_p=0.375µm (dashed curves) the highest cut off frequency is 97.9GHz, this is given for d_n=0.2µm and d_{abs}=0.1µm. Enlarging the depletion region produces low cutoff frequencies as illustrated in case of d_p=0.5µm (solid curves). The revealed cutoff frequency is 75.97GHz which is obtained when d_n=0.275µm and d_{abs}=0.1µm. However, figure.6.b affirms that high cutoff frequencies needs low thicknesses [52]. In this figure a very thin depletion region shows high cutoff frequencies (>160GHz).

To summarize this part, three situations are distinguished. For very thin depletion region, the capacitance effect attains its maximum since it is inversely proportional to the depletion region thickness while the transit time is very short. Enlarging the depletion region reduces gradually the capacitance effect and rises progressively the transit time. At this stage, the situation arrives to an equilibrium point between the capacitance effect and the transit time which enhances the cutoff frequency. Then, when the depletion region becomes sufficiently large, the capacitance effect diminishes while the transit time increases rapidly since it is directly proportional to the depletion region thickness. Consequently, the cutoff frequency leaves its maximum and decreases rapidly. These results show the dominance of the capacitance for thin depletion regions and the transit time for thick depletion regions, so there is a tradeoff between the transit time and the capacitance effect.

5. Comparative study

In order to reinforce the present work, this section focuses on the benefit of using p-i-n photodiode based InGaAsN lattice matched to GaAs having double transparent layers instead of single transparent layer or totally absorbent region.

The cutoff frequency (Fc) of p-i-n photodiode has been tackled in several works such as Ref [53] where author adopted three structures based on different depletion regions thicknesses. The results of comparison with this study are shown in figure.7.

The first structure is a conventional photodiode in which the depletion region is totally absorbent with a thickness of 0.8µm. The frequency response can be obtained by setting d_p and d_n to zero in equations 14 and 15. In our work F_c is equal to 74GHz, whereas in Ref [53] F_c=37GHz.

The second structure consists of single transparent layer placed on n-side of the absorbent region. Their thicknesses are 0.2 and 0.6µm respectively. Using the proposed structure, we have found F_c=69.60GHz, whereas in Ref [53] F_c=45GHz.

The last structure is organized as follow: double transparent layers inserted on n-side and p-side of a very thin absorbent region. Their thicknesses are respectively: d_n=0.45µm, d_p=0.35µm and d_{abs}=4nm. The exhibited cutoff frequency in our study is F_c=80.63GHz, whereas in Ref [53] F_c=62GHz.

Another comparison with literature results has been performed. Ref [27] adopted a conventional photodiode structure in which the absorbent region thickness is d_{abs}=1.5µm and the cutoff frequency was found 4GHz.

To accomplish this comparison, we have kept the absorbent region thickness at 1.5µm (d_{abs}=1.5µm), the results of this comparison are illustrated in figure.8 for d_p and d_n ranging from 0 to 0.4µm. From the obtained results we have selected some transparent layers thicknesses (found in section.4) that improve the photodiode response to show the influence of the transparent layers on the photodiode response.

In case d_p=0.375µm and d_n=0.2µm, the obtained cutoff frequency is about 51.5GHz, whereas, when d_p=0.125µm and d_n=0.2µm F_c reaches 56.2GHz. However, for d_p=0.15µm and d_n=0.2µm F_c is about 56.23GHz.

This section asserts that the p-i-n photodiode based InGaAsN lattice matched to GaAs using double transparent layers exhibits high-speed compared to both the conventional one and that whose depletion region consists of single transparent layer.

6. Capacitance effect

The capacitance is directly proportional to the area, but inversely to the depletion region thickness. It is given as [23, 26, 54-56]:

$$C = \varepsilon_o \cdot \varepsilon_r \cdot \frac{A}{d_t} \quad (16)$$

where

ε_o is the permittivity of free space,

ε_r is the relative permittivity of $In_xGa_{1-x}As_{1-y}N_y$. In case of x=0.06 and y=0.02 the relative permittivity is 12.95.

A is the junction area and d_t is the depletion region thickness.

Figure.9 illustrates the variation of the capacitance as a function of the depletion region thickness and the area. As shown in this figure, important capacitance is obtained for thin depletion regions and big areas. The variation of the capacitance with the depletion region thickness and the area is resumed in table.1.

According to table.1, structures whose depletion regions have thicknesses of d_{ti}; i=1…6 exhibit high capacitance by incrementing 'i'. Besides, this table shows the impact of the area on the capacitance. Areas of 100µm^2 show important capacitance compared to those given for areas of 25µm^2.

7. The total frequency response

This section is devoted to the total frequency response calculation and simulation with highlighting its limitations. The total cutoff frequency is given as [23,54,55]:

$$f_{3dB} = \frac{1}{\sqrt{f_{RC}^{-2} + f_t^{-2}}} \quad (17)$$

where

f_t : is the transit cutoff frequency which is related much more to the transit phenomenon.

f_{RC}: is the capacitive cutoff frequency, it is directly proportional to the depletion region thickness and inversely to the area. It is given as [23,26,54-56]:

$$f_{RC} = \frac{d_t}{2 \cdot \pi \cdot R \cdot \varepsilon_0 \cdot \varepsilon_r \cdot A} \quad (18)$$

Where, R is the photodiode total resistance and the load resistance.

The variation of the total cutoff frequency as function of d_n is presented in figure.10 (a,b,c) for different areas: 25, 50 and 100µm^2 using different depletion regions thicknesses: in (a) d_p=0.50µm and d_{abs}=0.1µm, in (b) d_p=0.375µm and d_{abs}=0.1µm and in (c) d_p=0.20µm and d_{abs}=0.1µm. The same is in figure.11 (a,b,c), it illustrates the variation of the total cutoff frequency depending on d_p for different areas: 25, 50 and 100µm^2 using different depletion regions thicknesses, for (a) d_n=0.20µm and d_{abs}=0.30µm, for (b) d_n=0.20µm and d_{abs}=0.20µm, and for (c) d_n=0.20µm and d_{abs}=0.10µm. The total cutoff frequency shows degradation when increasing the area from 25 to 50µm^2, this is due to the capacitance effect increases, which is directly proportional to the area. For areas ranging from 50 to 100µm^2 the capacitance effect increase considerably, thereby a severe degradation is observed in the total cutoff frequency.

The degradation is less important in figures 10.a and 10.b, however in figure 10.c the degradation is severe. In figure 10.a, area of 100µm^2 allows a degradation of 4% in the total cutoff frequency relative to area of 25µm^2. In figure 10.b, area of 100µm^2 allows a degradation of 10% in the total cutoff frequency relative to area

of 25µm^2, while in figure 10.c it is 35% relative to area of 25µm^2. The same is in figure 11; the degradation in the total cutoff frequency in both figures 11.a and 11.b is slight compared to figure 11.c. In figure 11.a, area of 100µm^2 allows a degradation of 11% in the total cutoff frequency relative to area of 25 µm^2. In figure 11.b, for A=100µm^2 the degradation is 18% in the total cutoff frequency relative to area of 25µm^2, while in figure 10.c it is 28% relative to area of 25µm^2. These results confirm the impact of increasing the area on the total frequency response.

Indeed, the total cutoff frequency depends not only on the area but also on the depletion region thickness, the latter influences more on the carriers' transit time than the capacitance. In figures 10.c, the degradation in total cutoff frequency is very important owing to the use of thin depletion region $d_{t,c}$. The latter produces short transit time compared to those thicknesses in figure 10.a and figure 10.b given as: $d_{t,a}$ and $d_{t,b}$ respectively. These two factors can be expressed as function of $d_{t,c}$ as follow: $d_{t,a} = 2.187d_{t,c}$ and $d_{t,b} = 1.687d_{t,c}$. The same observation is in figures 11. In figure 11.c the degradation in total cutoff frequency is very important due to the use of relatively thin depletion region $d'_{t,c}$ which engenders short transit time compared to $d'_{t,a}$ and $d'_{t,b}$ for figure 11.a figure 11.b respectively. These two thicknesses can be written as function of $d'_{t,c}$ as follow: $d'_{t,a} = 1.388d'_{t,c}$ and $d'_{t,b} = 1.166d'_{t,c}$.

Thus, using thin depletion regions and at the same time high areas increases the severity of degradation in the total cutoff frequency. Whereas, a relatively thick depletion regions ($d_{t,a}$, $d_{t,b}$ in figure 10 and $d'_{t,a}$, $d'_{t,b}$ in figure 11) make it possible to compensate the increase of the capacitance effect caused by increasing the area, thereby, reducing the severity of degradation in the total cutoff frequency.

On the other hand, very high speed responses need low thicknesses [33]. This can be observed if we compare for example blue curve (A=25 µm^2) of figure 10.a (or figure 11.a) with blue curve (A=25 µm^2) of figure 10.c (or figure 11.c). In figure 10.c (figure 11.c) the depletion region has low thickness and it exhibits high cutoff frequencies compared to figure 10.a (or figure 11.a) in which we have relatively thick depletion region.

In summary of these results, in figures 10 and 11, areas less than or equal 25µm^2 (blue curves) exhibit low capacitance effect. This fact increases significantly the capacitive cutoff frequency versus the transit one, thereby the total cut of frequency becomes strongly dominated by the transit cutoff frequency which related to the transit phenomenon, this dominance is as follow $f_{RC}/\sqrt{1+(f_{RC}/f_t)^2}$. By contrast, areas greater than 25µm^2 increase the capacitance effect, thereby, decrease the capacitive cutoff frequency. With increasing the area till 100µm^2, the capacitance effect becomes important which decreases significantly the capacitive cutoff frequency

versus the transit component. Thus, the total cutoff frequency becomes dominated by the capacitive cutoff frequency as in $f_t/\sqrt{1+(f_t/f_{RC})^2}$.

8. Conclusion

In this work, the lattice matched $In_xGa_{1-x}As_{1-y}N_y$/GaAs based pin photodiode whose depletion region consists of double transparent layers is proposed in order to improve the device performances. Besides, the link between the absorption coefficient and the device response has been tackled in order to select the suitable nitrogen and indium concentrations. For a concentration of nitrogen at 2.5% allows to get an absorption coefficient of $4.44x10^5 cm^{-1}$and an unchangeable cutoff frequency of about 67.46GHz regardless the absorbent region thickness. However, 2% of nitrogen leads to an absorption coefficient of about $4.72.10^4 cm^{-1}$ and an improvement in the cutoff frequency by varying the absorbent region thickness as follow: 42.86GHz for 1µm to 49.03GHz for 0.5µm and 59.00GHz for 0.2µm with keeping the transparent layers thicknesses d_p and d_n at 0.5µm. In addition, this study affirms that thin depletion regions make it possible to achieve cutoff frequencies (>100GHz). It has been also found that the total cutoff frequency completely depends on the transit cutoff frequency for areas less than $25\mu m^2$. Besides, the proposed structure is able to be adopted for ultra-high-speed applications.

References

[1]. M. Gladysiewicz, R. Kudrawiec, M. S. Wartak, Theoretical studies of optical gain tuning by hydrostatic pressure in GaInNAs/GaAs quantum wells, J. Appl. Phys. 115 (3) (2014) 1-9.

[2]. C. M. Duque, A. L. Morales, M. E. Mora-Ramos, C. A. Duque, Exciton-related nonlinear optical response and photoluminescence in dilute nitrogen $In_xGa_{1-x}N_yAs_{1-y}$/GaAs cylindrically shaped quantum dots, J. Lumin. 154 (2014) 559-568.

[3]. M. Gladysiewicz, R. Kudrawiec, M. S. Wartak, Material gain in $Ga_{0.66}In_{0.34}N_yAs_{1-y}$, $GaN_yAs_{0.69-y}Sb_{0.31}$, and $GaN_yP_{0.46}Sb_{0.54-y}$ comparative theoretical studies, IEEE J. Quant. Electron. 50 (12) (2014) 996-1005.

[4]. I. Mal, D. P. Samajdar. A. J. Peter, Theoretical studies on band structure and optical gain of GnInAsN/GaAs cylindrical quantum dot, Superlattices Microst. 119 (2018) 103-113.

[5]. K. A. Mohamad, M. S. Nordin, N. Nayan, A. Alias, A. R. Mohmad, A. Boland-Thomas, A.J. Vickers, Characterization of III-V dilute nitride based multi-quantum well p-i-n photodiodes for next generation opto-electrical conversion devices, Mater. Today. Proc. 7 (Part 2) (2019) 625-631.

[6]. E.-M. Pavelescu, N. Baltateanu, S. I. Spanulescu, E. Arola, Very high dose electron irradiation effects on photoluminescence from GaInNAs/GaAs quantum wells by molecular beam epitaxy, Opt. Mater. 64 (2017) 361-365.

[7]. F. Sarcan, F. Nutku, O. Donmez, F. Kuruoglu, S. Mutlu, S. Yildirim, M. C. Arikan, Quantum oscillations and interference effects in strained n-and p-type modulation doped GaInNAs/GaAs quantum wells, J. Phys. D. Appl. Phys. IOP Publishing. 48 (30) (2015) 1-9.

[8]. K. Nomura, T. Yamada, Y. Iguchi, S. Takagishi, M. Nakayama, Photoluminescence properties of localized states caused by nitrogen alloying in a GaInNAs/GaAs single quantum well, J. Lumin. 112 (1-4) (2005) 146-150.

[9]. F. Ungan, S. Sakiroglu, U. Yesilgul, A. Erol, E. Kasapoglu, H. Sari, I. Sokmen, Effects of indium and nitrogen mole concentrations on the optical properties in a GaInNAs/GaAs quantum well under the intense laser field, J. Lumin. 134 (2013) 208-2012.

[10]. J. F. Geisz, D. J. Friedman, III–N–V semiconductors for solar photovoltaic applications, Semicond. Sci. Technol. 17 (8) (2002) 769–777.

[11]. A. Kosa, L. Stuchlikova, L. Harmatha, M. Mikolasek, J. Kovac, B. Sciana, W. Dawidowski, D. Radziewicz, M. Tlaczala, Defect distribution in InGaAsN/GaAs multilayer solar cells. 132 (2016) 587-590.

[12]. S. R. Kurtz, A. A. Allerman, E. D. Jones, J. M. Gee, J. J. Banas, and B. E. Hammons, InGaAsN solar cells with 1.0 eV band gap, lattice matched to GaAs, Appl. Phys. Lett. 74 (5) (1999) 729-731.

[13]. A. Aissat , R. Bestam , B. Alshehri , J. P. Vilcot, Modeling of the absorption properties of $Ga_{1-x}In_xAs_{1-y}N_y$ quantum well structures for photodetection applications, Superlattices Microst. 82 (2015) 623–629.

[14]. M. Kondow, K. Uomi, A. Niwa, T. Kitatani, S. Watahiki, Y. Yazawa, GaInAsN: a novel material for long-wavelength-range laser diodes in the excellent high-temperature performance, Jpn. J. Appl. Phys. 35 (1996) 1273–1275.

[15]. I. Mal, J. Jayarubi, S. Das, A. S. Sharma, A. J. Peter, D. P. Samajdar, Hydrostatic pressure dependent optoelectronic properties of InGaAsN/GaAs spherical quantum dots for laser diode application, Phys. Status Solidi B. 256 (3) (2018) 1-13.

[16]. S. Sato, S. Satoh, Metalorganic chemical vapor deposition of GaInNAs lattice matched to GaAs for long-wavelength laser diodes, J. Cryst. Growth. 192 (3-4) (1998) 381-385.

[17]. S. Sato,Y.Osawa, T. Saitoh, Room-temperature operation of GaInAsN/GaInP double-heterostructure laser diodes grown by Metalorganic chemical vapor deposition, Jpn. J. Appl. Phys. 36 (1997) 2671-2675.

[18]. L. Bellaiche, Band gaps of lattice-matched (Ga,In)(As,N) alloys, Appl. Phys. Lett. 75 (17) (1999) 2578-2580.

[19]. Y. Park, M. J. Cich, R. Zhao, P. Specht, H. Feick, E. R. Weber, AFM study of lattice matched and strained InGaAsN layers on GaAs, Phys. B: 308–310 (2001) 98–101.

[20]. L. J. J. Tan, W. M. Soong, J. P. R. David, J. S. Ng, Dark Current Mechanism in Bulk GaInNAs Lattice matched to GaAs, IEEE Trans. Electron Devices. 58 (1) (2011) 103-106.

[21]. B. Royall, H. Khalil, S. Mazzucato, A. Erol, N. Balkan, Experimental investigation and numerical modelling of photocurrent oscillation in lattice matched $Ga_{1-x}In_xN_yAs_{1-y}$/GaAs quantum well p-i-n photodiodes, Nanoscale Res. Lett. 9 (1) (2014) 2-8.

[22]. S. T. Ng, W. M. Soong, M. J. Street, M. Hopkinson, J. P. R. David, J. Chamings, S. J. Sweeney, A. R. Adams, Long wavelength bulk GaInNAs p-i-n photodiodes lattice matched to GaAs, J. Appl. Phys. 101 (6) (2007) 1-6.

[23]. M. El Besseghi, A. Aissat, B. Alshehri, K. Dogheche, E.H. Dogheche, D. Decoster, Frequency response modeling and optimization of a PIN photodiode based on GaN/InGaN adapted to photodetection at a wavelength of 633 nm, Mater. Chem. Phys.162 (2015) 525-530.

[24]. R. Sabella, S. Merli, Analysis of InGaAs p-i-n photodiode frequency response, IEEE J. Quantum Electron. 29 (3) (1993) 906-916.

[25]. K. Konno, O. Matsushima, D. Navarro, M. Miura-Mattausch, High frequency response of p-i-n photodiodes analyzed by an analytical model in Fourier space, J. Appl. Phys. 96 (7) (2004) 3839-3844.

[26]. B. Alshehri, K. Dogheche, S. Belahsene, A. Ramdane, G. Patriache, D. Decoster, E. Dogheche, Dynamic Characterization of III-nitride base high speed photodiodes, IEEE Photonics J. 9 (4) (2017) 1-7.

[27]. M. Elbar, B. Alshehri, S.Tobbeche, E. Dogheche, Design and simulation of InGaN/GaN p–i–n photodiodes, Phys. Status Solidi a. 215 (9) (2018) 1-6.

[28]. G. Torrese, A. Salamone, I. Huynen, A. Vander Vorst, A fully analytical model to describe the high-frequency behavior of p-i-n photodiodes, Microw. Opt. Technol. Lett. 31 (5) (2001) 329-333.

[29]. S. Loquai, C.A. Bunge, O. Ziemann, B. Schmauss, R. Kruglov, A fully analytic model of large area silicon p-i-n photodiodes verified at short wavelengths, J. Lightwave Technol. 28 (18) (2010) 2646-2653.

[30]. F. J. Effenberger, A. M. Joshi. Ultrafast, dual-depletion region, InGaAs/InP p-i-n detector, J. Lightwave Technol. 14 (8) (1996) 1859-1864.

[31]. J. M. Torres. Pereira, J. P. N. Torres, Frequency response optimization of dual depletion InGaAs/InP pin photodiodes, Photonic Sens. 6 (1) (2016) 63-70.

[32]. G. Locovsky, R. F. Schwartz, R. B. Emmons, Transit time considerations in p-i-n diodes, J. Appl. Phys. 35 (3) (1964) 622-628.

[33]. D. Decoster, J. P. Vilcot, J. Harari, V. Magnin, Photodetectors for microwave applications: A revew and trends. in Proc. SPIE. 2003.

[34]. A. Aissat, A. Djili, S. Zelazel, and J. P. Vilcot, Modeling the structure based on GaAsNBi/GaAs for solar cell, Progress in Clean Energy. 1 (2015) 475-483.

[35]. L. Chenini, A. Aissat, J. P. Vilcot, Optimization of inter-subband absorption of InGaAsSb/GaAs quantum wells structure, Superlattices Microst. 129 (2019) 115-123.

[36]. E.-M. Pavelescu, R. Kudrawiec, J. Puustinen, A. Tukiainen, M. Guina, Effects of 7- MeV electron irradiation on photoluminescence from 1-eV GaInNAs-on-GaAs epilayers, J. Lumin. 136 (2013) 347-350.

[37]. C. Skierbiszewski, P. Perlin, P. Wisniewski, T. Suski, J. F. Geisz, K. Hingerl, W. Jantsch, D. E. Mars, W. Walukiewicz, Band structure and optical properties of $In_yGa_{1-y}As_{1-x}N_x$ alloys, Phys. Rev. B. 65 (3) (2001) 1-10.

[38]. M. Gladysiewicz, R. Kudrawiec, J. M. Miloszewski, P. Weetman, J. Misiewicz, M. S. Wartak. Band structure and the optical gain of GaInNAs/GaAs quantum wells modeled within 10-band and 8-band k.p model, J. Appl. Phys. 113 (6) (2013) 1-11.

[39]. Q. X. Zhao, S. M. Wang, M. Sadeghi, A. Larsson, M. Willander, and J. H. Yang, Effects of nitrogen incorporation on the properties of GaInNAs/GaAs quantum well Structures, J. Appl. Phys. 97 (7) (2005) 1-6.

[40]. W. Shan, W. Walukiewicz, J. W. Ager, E. E. Haller, J. F. Geisz, D. J. Friedman, J. M. Olson, and S. R. Kurtz, Band Anti-Crossing in GaInNAs alloys, Phys. Rev. Lett. 82 (6) (1999) 1221- 2124.

[41]. K. Koksal, M. S¸ahin, The effect of dilute nitrogen on nonlinear optical properties of the InGaAsN/GaAs single quantum wells, Eur. Phys. J. B 85 (10) (2012) 2-8.

[42]. A. Aissat, S. Nacer, M. Seghilani, J. P. Vilcot, Effect of on band alignment of compressively strained $Ga_{1-x}In_xN_yAs_{1-y-z}Sb_z$/GaAs quantum well structures, Physica E: 43 (1) (2010) 40–44.

[43]. S. T. Ng, W. J. Fan, Y. X. Dang, S. F. Yoon, Comparison of electronic band structure and optical transparency conditions of $In_xGa_{1-x}As_{1-y}N_y$/GaAs quantum wells calculated by 10-band, 8-band, and 6-band k·p models, Phys. Rev. B 72 (11) (2005) 1-13.

[44]. A. Aissat, R. Bestam, H. Arbouz, J. P. Vilcot, Efficiency Improvement of the Structure InGaN/GaN for Solar cells Applications. Proceedings of the 3rd international renewable and sustainable energy conference (IRSEC), Marrakech (2015) 1-4.

[45]. R. Bestam, A. Aissat, J. P. Vilcot, High efficiency quadruple junction solar cells, Superlattices Microst. 91 (2016) 22-30.

[46]. V. Palankovsky, Simulation of heterojunction bipolar transistor, for obtaining the academic degree: a doctor of technical sciences, Faculty of electrical engineering and information technology, University of technology, Vienna, December 2000.

[47]. R.Quay, Analysis and simulation of high electron mobility transistors, for obtaining the academic degree: a doctor of technical sciences, Institute of microelectronics, E360, Faculty of electrical engineering and information technology, University of technology, Vienna, July 2001.

[48]. S. Adachi, Properties of group-IV, III–V and II–VI semiconductors, John Wiley & Sons, England 2005.

[49]. J. Piprek, Semiconductor Optoelectronic Devices: Introduction to Physics and Simulation, Academic Press: San Diego, 2003.

[50]. R. Quay, Gallium nitride electronics, Germany, Berlin: Springer-Verlag, 2008.

[51]. J. Piprek, Nitride semiconductor devices: principles and simulation, Wiley-VCH, Weinheim, 2007.

[52]. K. Kato, Ultrawide-band/high-frequency photodetectors, IEEE Trans. Microw. Theory Tech. 47 (7 PART 2) (1999) 1265-1281

[53]. A. Aissat, M. El Besseghi, D. Decoster, Transport optimization in pin photodiodes using mixed depletion region, Int. J. Electron. Lett. 3 (3) (2014)160-169.

[54]. Z. Yang, High-Power Photodiodes and their Application in Analog Photonic Links, Doctor of Philosophy, university of Virginia, electrical engineering, school of engineering and applied science, April 2018.

[55]. Z. Xu, S. F. Yoon, W. K. Loke, C. Y. Ngo, K. H. Tan, S. Wicaksono, N. Saadsaoud, D. Decoster, M. Zegaoui, J. Chazelas. Design considerations for 1.3µmGaNAsSb-GaAs high speed and high quantum efficiency waveguide photodetectors, J. Lightwave Technology. 27 (13) (2009) 2518-2524.

[56]. D. Decoster, J. Harari, Optoelectronics sensors, ISTE Ltd and Jhon Wiley & Sons, Inc, 2009.

Figure captions

Figure.1. Variation of the strain versus the indium and nitrogen concentrations, we are interested in $\varepsilon(x,y)=0$.

Figure.2. Variation of the absorption coefficient versus nitrogen concentration using different indium concentrations providing some nitrogen concentrations for the stable structure and E=1.08eV.

Figure.3. Structure of the proposed InGaAsN/GaAs p-i-n photodiode.

Figure.4. Frequency response simulationfor$In_{0.06}Ga_{0.94}As_{0.98}N_{0.02}$/GaAs p-i-n photodiode depending on different absorbent region thicknesses, d_p and d_n are kept at 0.50µm.

Figure.5. Variation of the cutoff frequency as a function of the p-side transparent layer thickness using different absorbent region thicknesses ;d_n=0.20µm for dashed curves and 0.50µm for solid curves.

Figure.6. (a, b). Variation of the cutoff frequency as a function of the n-side transparent layer thickness using different absorbent region thicknesses, a)d_p=0.375µm for dashed curves and 0.5µmfor solid curves.

b) d_p=0.20µm.

Figure.7. Frequency response of the$In_{0.06}Ga_{0.94}As_{0.98}N_{0.02}$/GaAs p-i-n photodiode for different depletion region thicknesses compared to that in Ref [53]..

Figure.8. Frequency response variation of the $In_{0.06}Ga_{0.94}As_{0.98}N_{0.02}$/GaAs p-i-n photodiode for d_{abs}=1.50µm.

Figure.9. Variation of the capacitance as a function of the n-side and p-side transparent layers thicknesses. The area A is 25µm^2 and 100µm^2 and the absorbent region thickness d_{abs} is 0.1µm and 0.3µm.

Figure.10. (a,b, c)Variation of the total cutoff frequency as a function of n-side transparent layer thickness using different areas, a) d_p=0.50µm and d_{abs}=0.10µm, b) d_p=0.375µm and d_{abs}=0.10µm, c) d_p=0.20µm and d_{abs}=0.10µm.

Figure.11. (a,b,c).Variation of the total cutoff frequency as a function of p-side transparent layer thickness using different areas, d_n=0.20µm and d_{abs}=0.30µm, b) d_n=0.20µm and d_{abs}=0.20µm, c) d_n=0.20µm and d_{abs}=0.10µm.

Table.1. Impact of the area and the depletion region thickness on the capacitance.

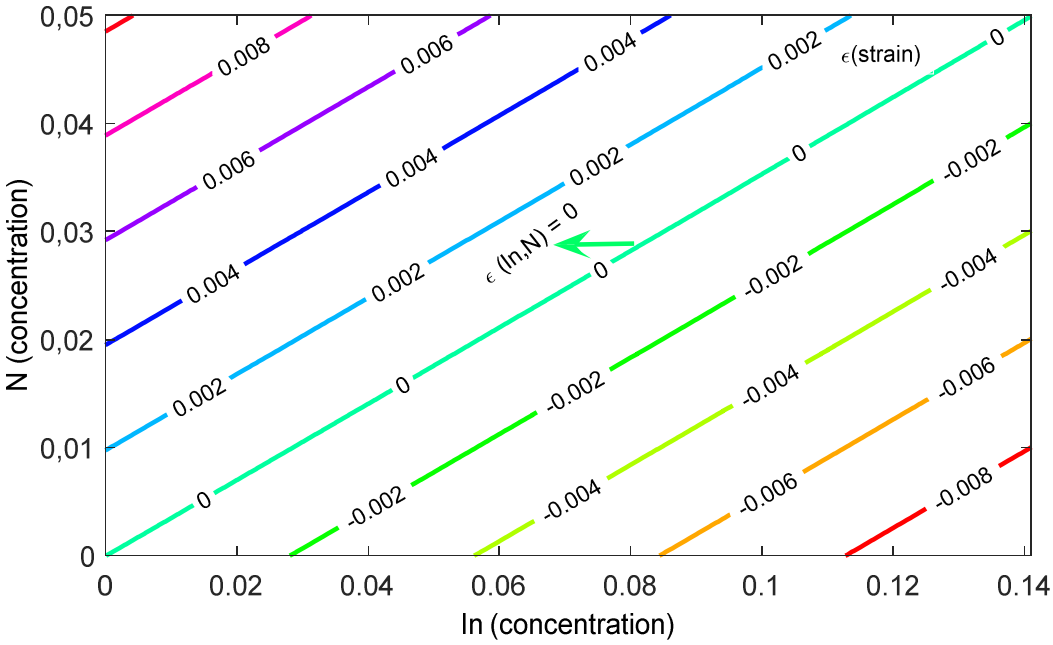

Figure 1

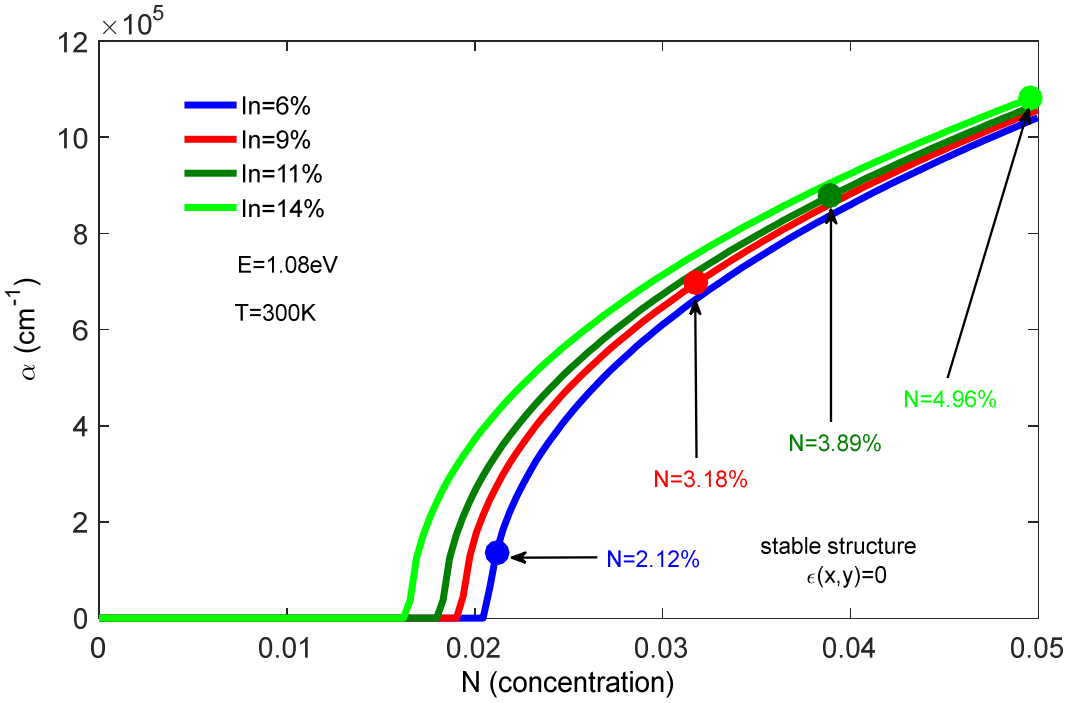

Figure 2

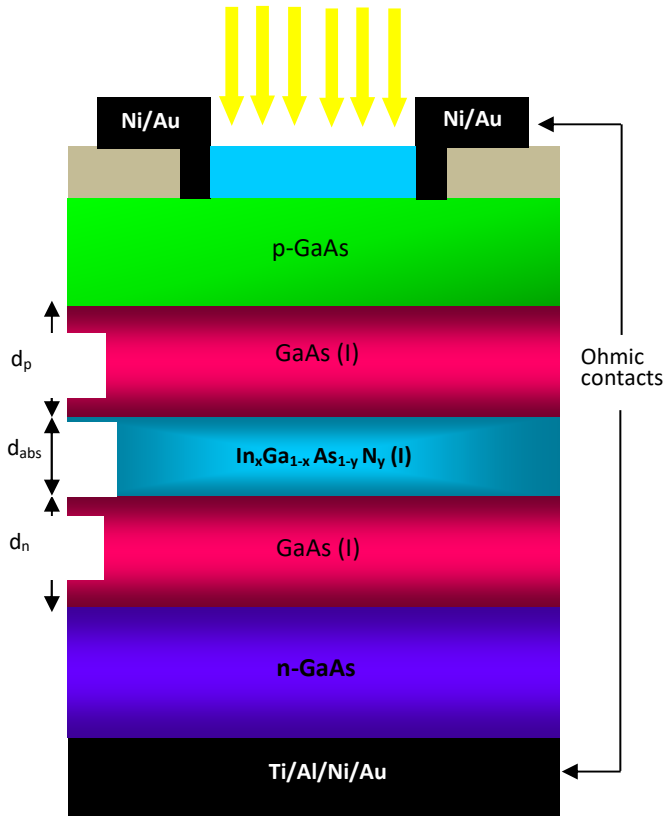

Figure 3

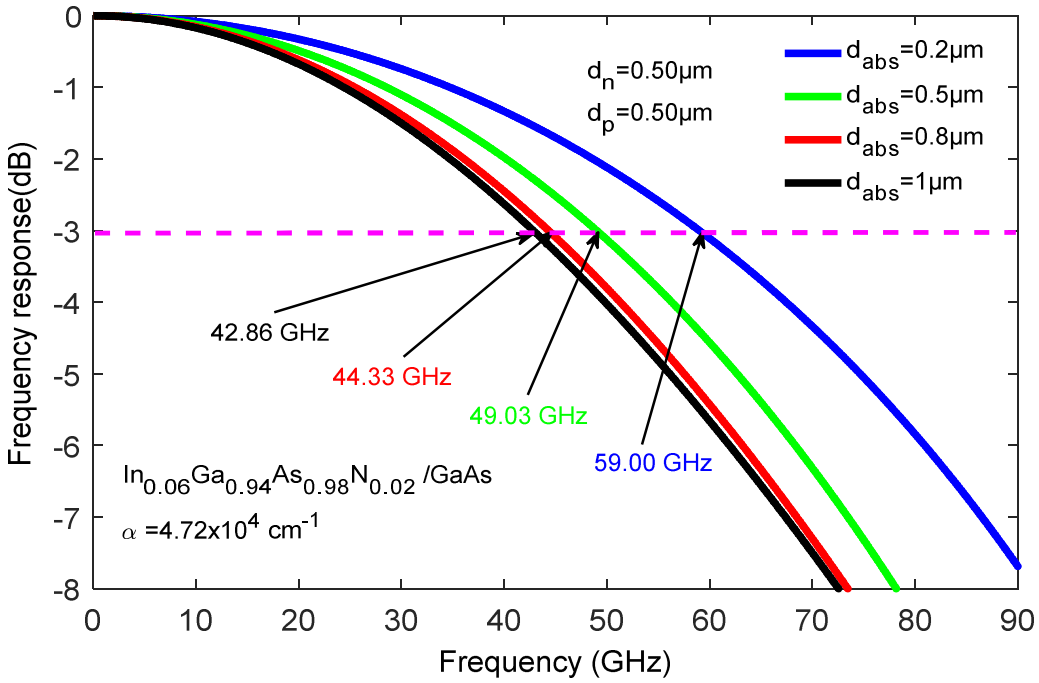

Figure 4

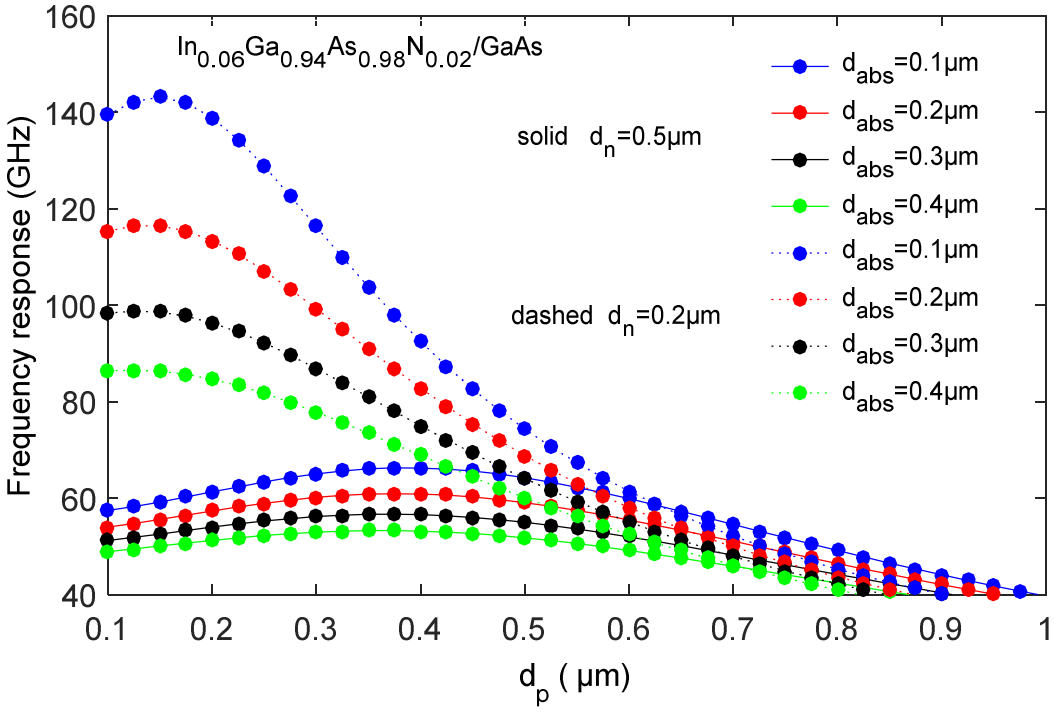

Figure 5

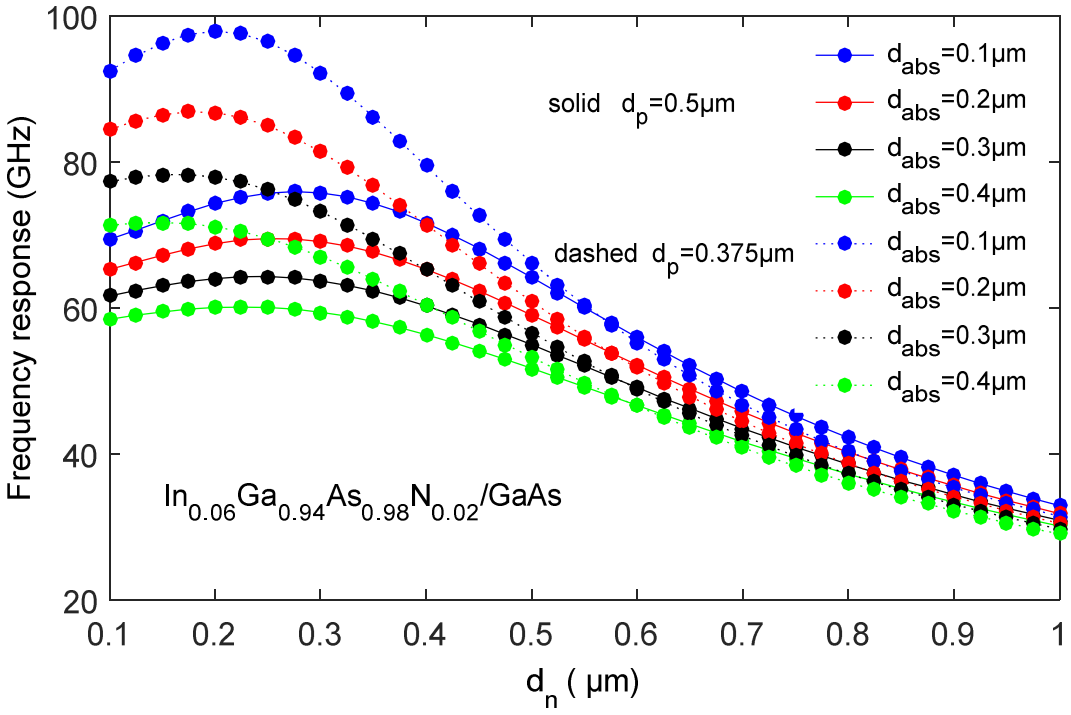

Figure 6.a

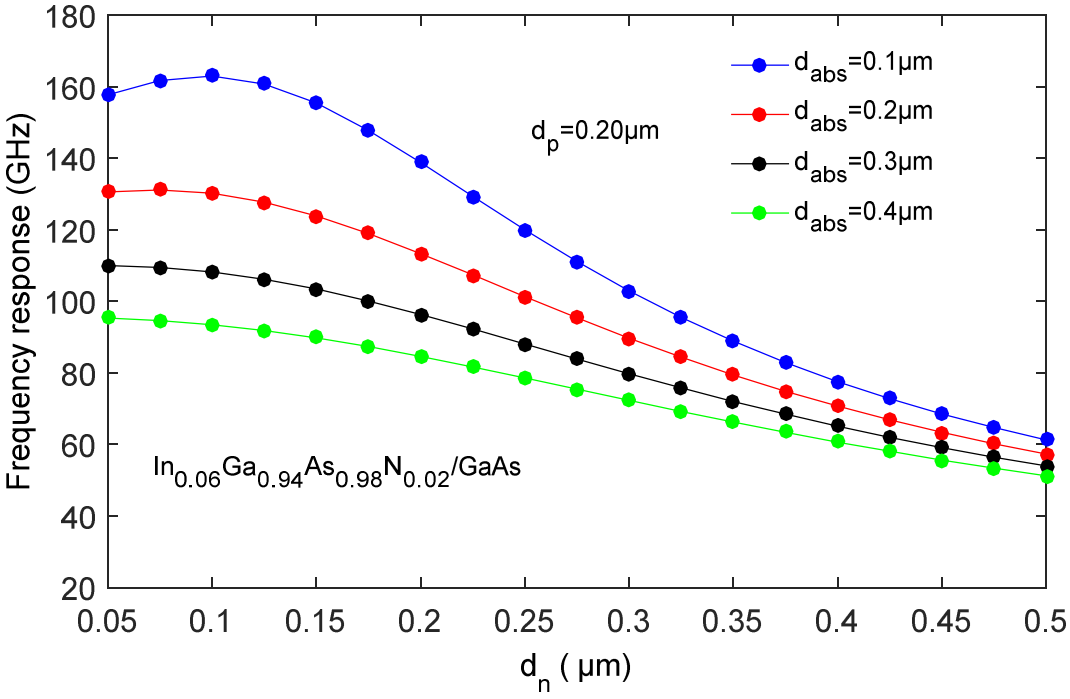

Figure 6 .b

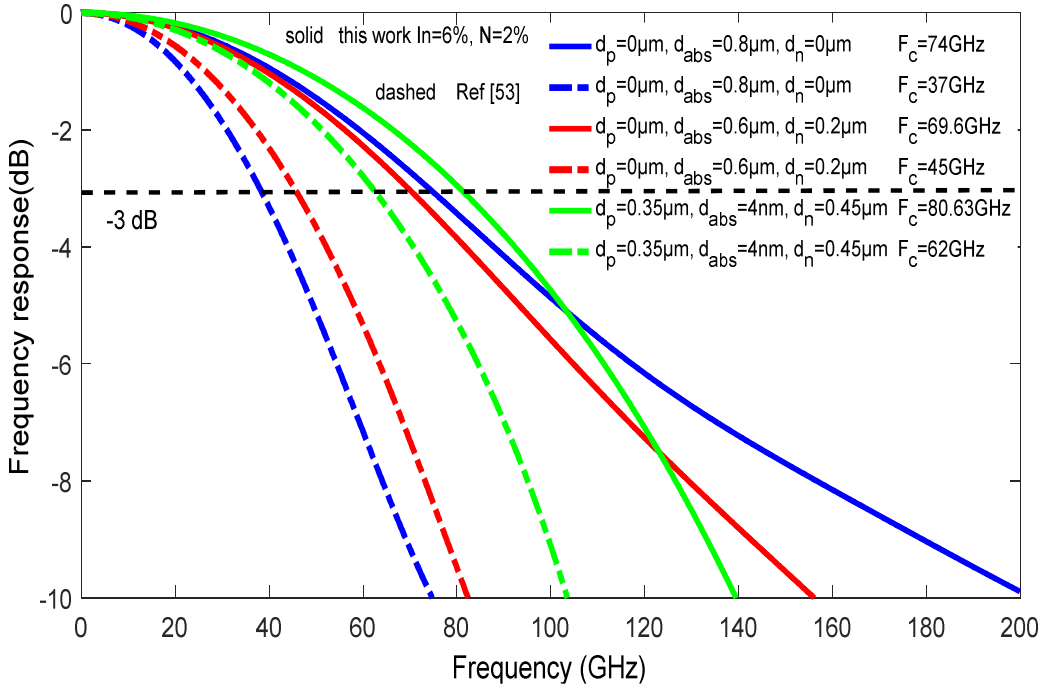

Figure 7

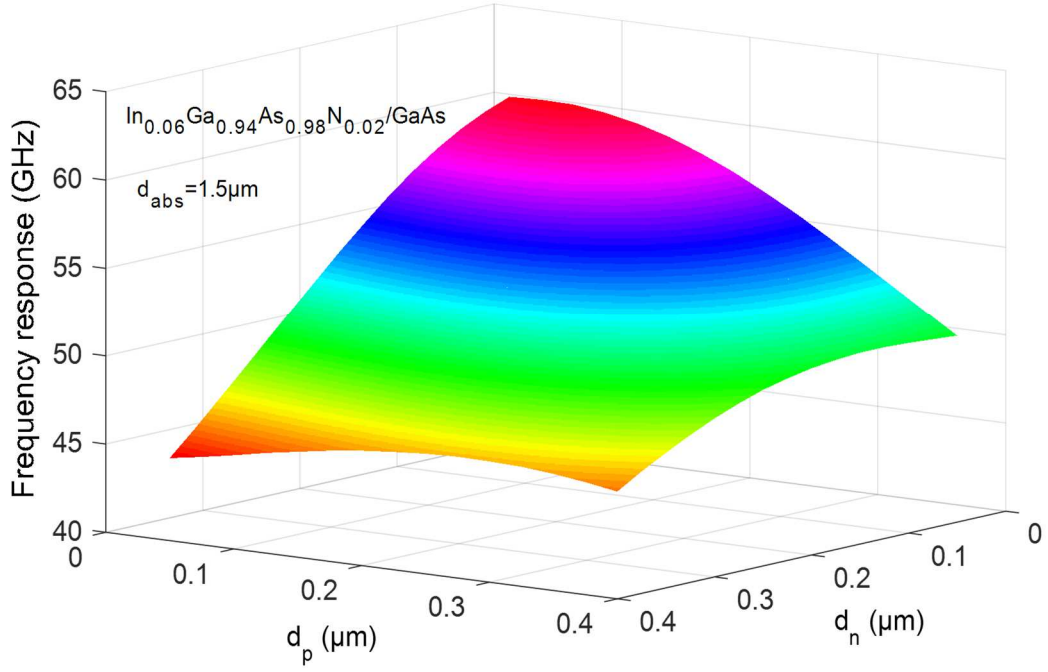

Figure 8

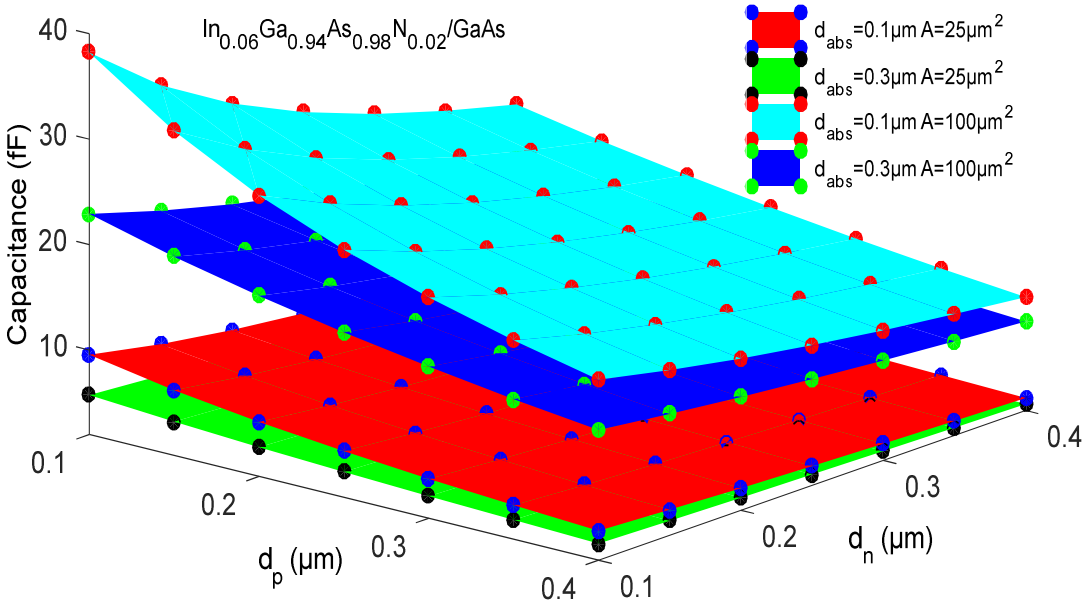

Figure 9

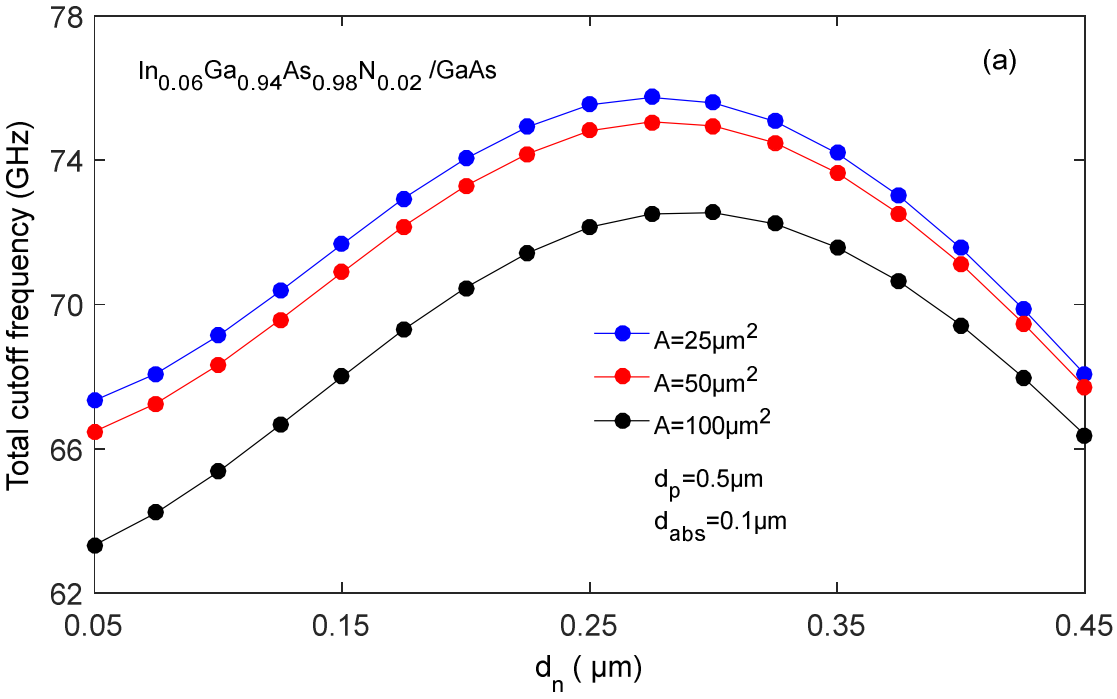

Figure 10.a

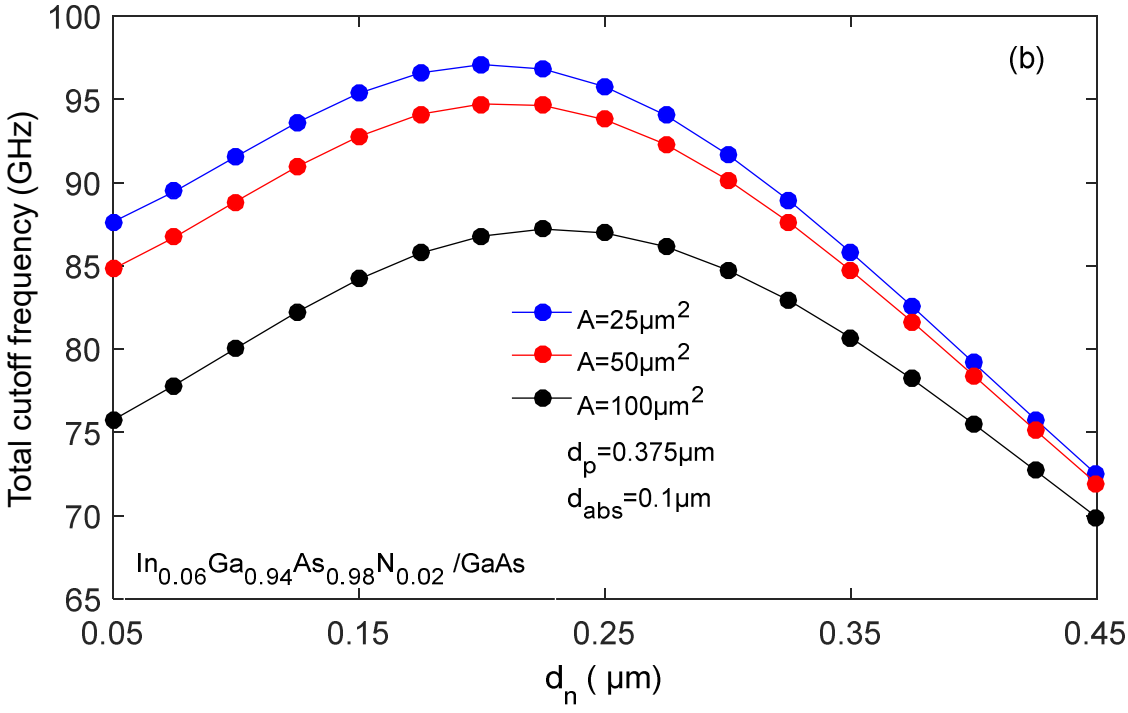

Figure 10.b

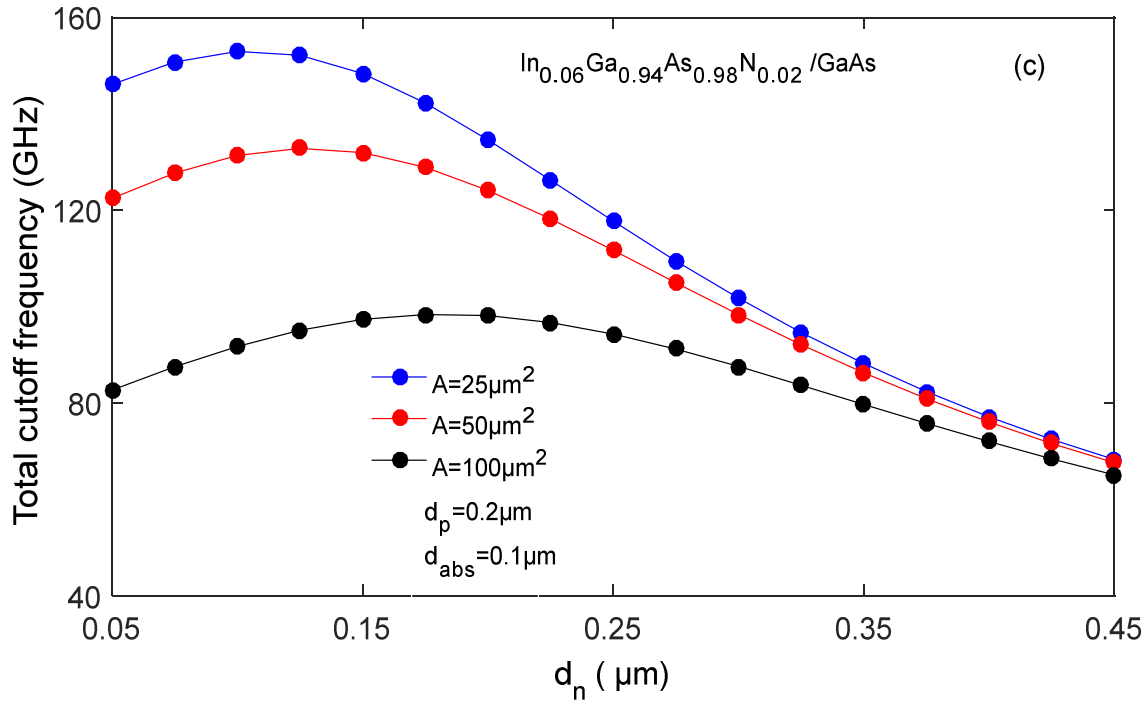

Figure 10. c

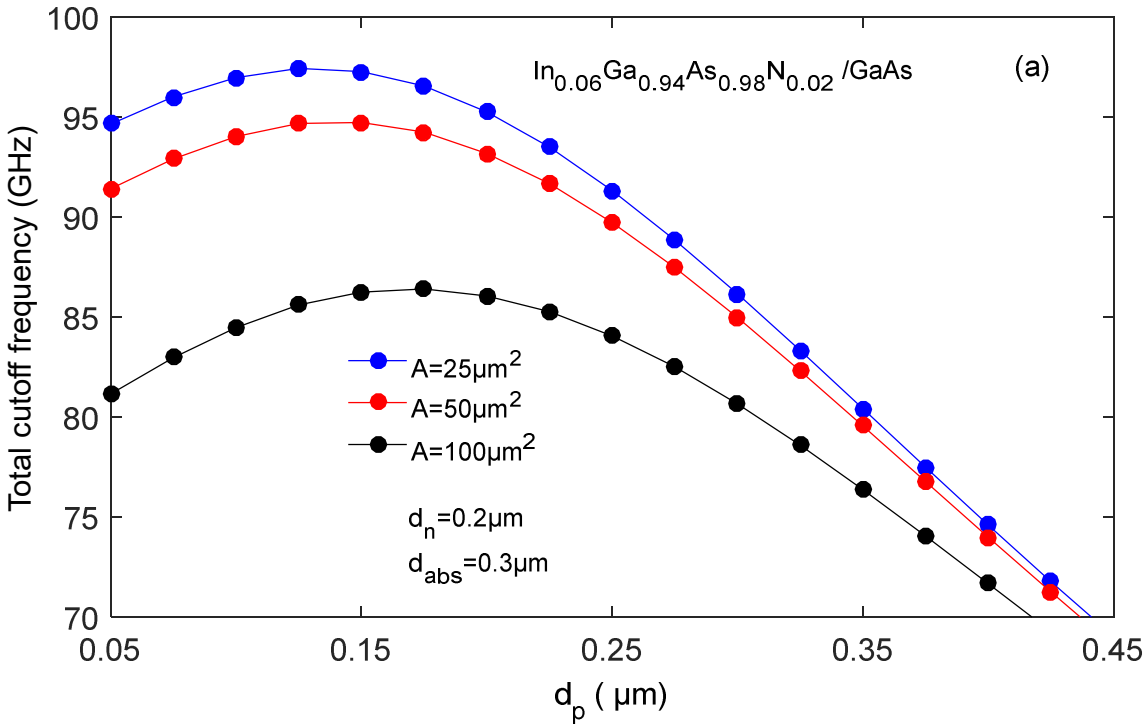

Figure 11.a

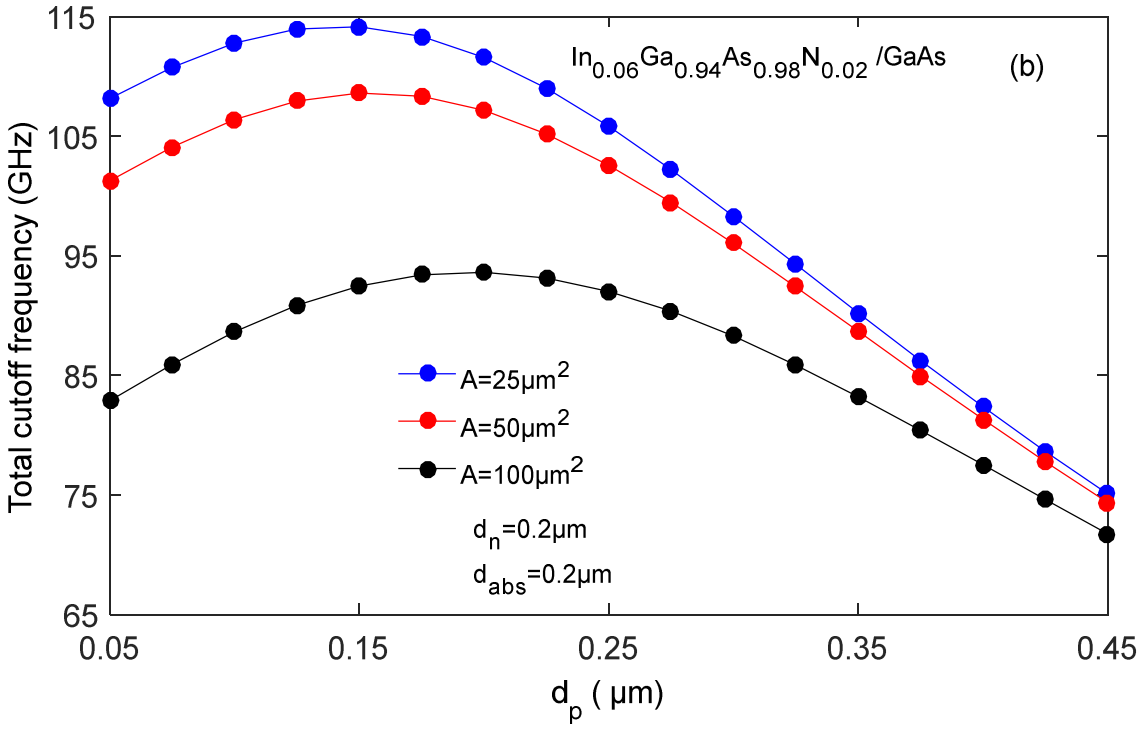

Figure 11.b

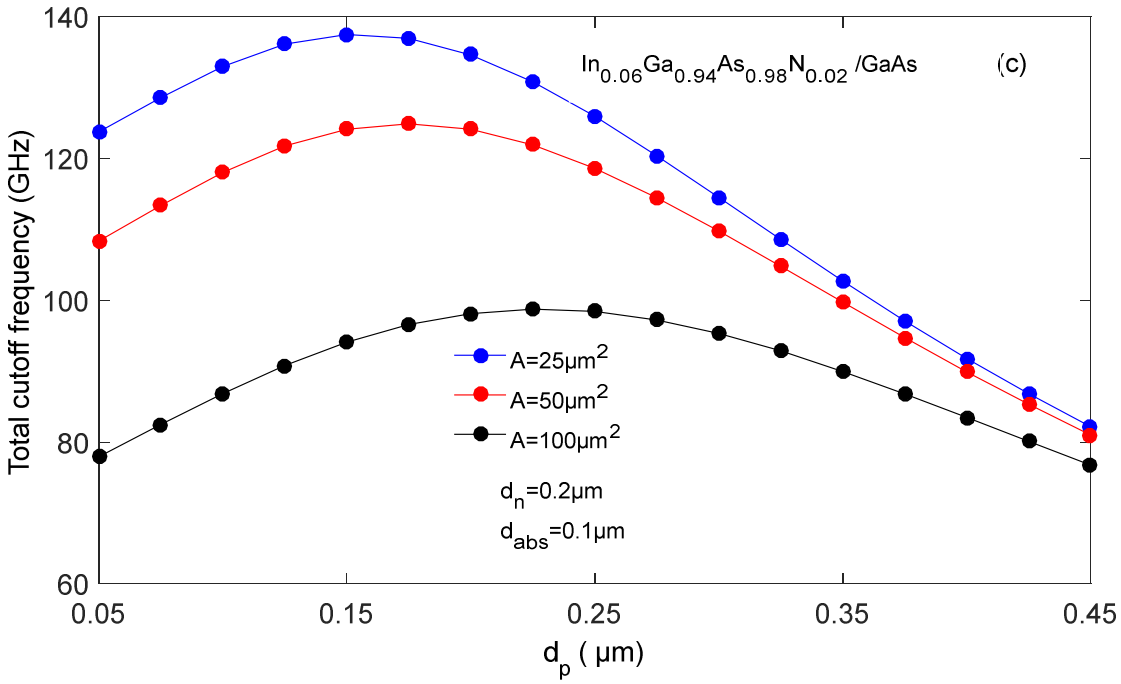

Figure 11.c

Table.1

		$A=25\mu m^2$	$A=100\mu m^2$
dti, depletion region thickness (μm)		Capacity (fF)	Capacity (fF)
$d_{t1}=0.875$	$d_p=0.5$, $d_n=0.275$ and $d_{abs}=0.1$	3.27	13.1
$d_{t2}=0.675$	$d_p=0.375$, $d_n=0.2$ and $d_{abs}=0.1$	4.24	16.98
$d_{t3}=0.625$	$d_p=0.125$, $d_n=0.2$ and $d_{abs}=0.3$	4.58	18.34
$d_{t4}=0.55$	$d_p=0.15$, $d_n=0.2$ and $d_{abs}=0.2$	5.21	20.85
$d_{t5}=0.45$	$d_p=0.15$, $d_n=0.2$ and $d_{abs}=0.1$	6.37	25.48
$d_{t6}=0.4$	$d_p=0.2$, $d_n=0.1$ and $d_{abs}=0.1$	7.16	28.66